J Solid State Electrochem (2012) 16:545–550
DOI 10.1007/s10008-011-1378-8

ORIGINAL PAPER

Nanostructured PdRu/C catalysts for formic acid oxidation

Zhaolin Liu · Xinhui Zhang · Siok Wei Tay

Received: 20 September 2010 / Revised: 4 March 2011 / Accepted: 13 March 2011 / Published online: 12 April 2011

Abstract Pd and bimetallic PdRu nanoparticles supported on Vulcan XC-72 carbon prepared by the microwave-assisted polyol process are examined as electrocatalysts for the electrooxidation of formic acid. The catalysts are characterized by transmission electron microscopy and X-ray diffraction. The Pd and PdRu nanoparticles with sizes of <10 nm display the characteristic diffraction peaks of a Pd face-centered cubic (fcc) crystal structure. It is found that the addition of Ru to Pd/C can decrease the lattice parameter of Pd (fcc) crystal. The electrocatalytic activities of the catalysts are evaluated in sulfuric acid solution containing 1 M formic acid using linear sweeping voltammetry and chronoamperometry. The results show that Pd_5Ru_1/C displays the best electrocatalytic performance among all catalysts for formic acid electrooxidation.

Keywords Carbon-supported PdRu nanoparticles · Palladium nanoparticles · Catalytic activity · Formic acid oxidation

Introduction

Direct methanol fuel cell (DMFC) has been widely studied and considered as possible power sources for the portable electronic devices and electric vehicles during the past 20 years. These fuel cells offer a variety of benefits such as high specific energy and the ready availability and portability of methanol. However, DMFC has some serious disadvantages [1]. Firstly, the methanol "crossover" from the anode to the cathode through membrane leads to the waste of methanol and the decrease in the DMFC performance. Secondly, the anode catalyst Pt in DMFC is easy to be poisoned with CO. Thirdly, the use of methanol is not safe because methanol is a toxic, evaporable, and burnable compound. Recently, many advantages of direct formic acid fuel cell (DFAFC) have been recognized [2, 3]. For example, formic acid is non-toxic and not inflammable. Hsing and co workers [4] have reported that the rate of formic acid crossover can be reduced by five times, and a higher performance can be rendered by formic acid when compared to methanol under the same conditions.

It was reported that the electrooxidation of formic acid could undergo through two parallel pathways, the direct pathway and CO pathway [5–7]. In the direct pathway, formic acid is directly oxidized to CO_2. In the CO pathway, formic acid first adsorbs onto the catalyst surface, forming an intermediate adsorbed CO species by dehydration, which is then oxidized to CO_2. Carbon-supported Pt catalysts for electrooxidation of formic acid are poisoned severely by the adsorbed CO intermediate of the reaction [8–10]. The electrooxidation rate of formic acid at the Pt catalyst is insufficient for the practical application, because the electrooxidation of formic acid at the Pt catalyst is mainly through the CO pathway. It has been demonstrated [11, 12] that PtRu and PtPd alloys can diminish this CO poisoning effect to some extent, but it still limits significantly the catalytic activity for formic acid oxidation. Recently, Masel et al. [13, 14] have disclosed that unsupported Pd and Pd/C catalysts can overcome CO poisoning effect and thereby yield high performances in the DFAFC. In order to further improve the electrocatalytic performance of the Pd and Pd/C catalysts, the Pd-based bimetallic catalysts, such as Pd-Ni [15], Pd-Au [16], Pd-Pt [17], and Pd-Ir [18], have

Z. Liu (✉) · X. Zhang · S. W. Tay
Institute of Materials Research and Engineering, Agency for Science, Technology and Research (A*STAR), 3 Research Link, Singapore 117602, Singapore
e-mail: zl-liu@imre.a-star.edu.sg

been investigated. However, to the best of our knowledge, PdRu bimetallic catalysts for formic acid electrooxidation have not been reported yet.

In this paper, PdRu nanoparticles are synthesized by a simple microwave-assisted polyol procedure and deposited on carbon to produce carbon-supported PdRu catalysts, aiming to have a less expensive electrocatalyst in the DFAFC. The physicochemical properties and electrochemical activities of the nanoparticles for formic acid oxidation are investigated. The reasons of oxidation activity enhancement for PdRu catalysts are discussed in detail.

Experimental

The Pd_aRu_b/carbon black (Cabot Vulcan XC-72, subscript denotes the atomic ratios of the alloying metal) catalysts were prepared by microwave heating of ethylene glycol (EG) solutions of $PdCl_2$ and $RuCl_3$ [19–21]. The Pd and Ru contents in each sample were 20 wt.%, 0.99, 1.5, and 3.0 mL of 0.02 M $RuCl_3$ (Aldrich, A.C.S. Reagent) and 4.9, 4.5, and 3.0 mL of 0.02 M $PdCl_2$ (Aldrich, A.C.S. Reagent) were chosen to yield Pd_5Ru_1/C, Pd_3Ru_1/C, and Pd_1Ru_1/C, respectively. A typical preparation of Pd_5Ru_1/C catalyst would consist of the following steps: 4.9 mL of 0.02 M $PdCl_2$ and 0.99 mL of 0.02 M $RuCl_3$ was mixed with 30 ml of ethylene glycol (Mallinckrodt, AR); 0.5 mL of 0.8 M NaOH was added dropwise; 0.05 g of Vulcan XC-72 carbon with a specific BET surface area of 250 $m^2\ g^{-1}$ and an average particle size of 40 nm was added to the mixture and sonicated. The solution was placed in a CEM "Discover" microwave reactor (CEM Corporation) with the maximum temperature set at 170 °C at atmospheric conditions for 30 s. The resulting suspension was filtered; and the residue was washed with acetone and dried at 100 °C over night in a vacuum oven. For comparison, Pd/C catalyst (20 wt.% Pd loading) was also prepared using the same method.

The catalysts were examined by TEM on a JEOL JEM 2010. For microscopic examinations, the samples were first ultrasonicated in acetone for 1 h and then deposited on 3 mm Cu grids covered with a continuous carbon film. X-ray diffraction (XRD) patterns were recorded by a Bruker GADDS diffractometer with area detector using a CuKα source (λ=1.54056 Å) operating at 40 kV and 40 mA. The samples were prepared by depositing carbon-supported nanoparticles on a glass slide.

An AUTOLAB potentiostat/galvanostat and a conventional three-electrode test cell were used for electrochemical measurements. The working electrode was a thin layer of Nafion-impregnated catalyst cast on a vitreous carbon disk held in a Teflon cylinder. The catalyst layer was obtained in the following way: (1) a slurry was first prepared by sonicating for 1 h a mixture of 0.5 ml of deionized water, 13 mg of Pd/C or PdRu/C catalyst, and 0.2 ml of Nafion solution (Aldrich, 5 wt.% Nafion); (2) 4 μl of the slurry was pipetted and spread on the carbon disk; (3) the electrode was then dried at 90 °C for 1 h and mounted on a stainless steel support. The surface area of the vitreous carbon disk was 0.25 cm^2 and the loading of the catalyst on the carbon disk electrode is 0.074±0.002 mg. Pt gauze and an Ag/AgCl electrode were used as the counter and reference electrodes, respectively. All potentials in this report are quoted against Ag/AgCl. All electrolyte solutions were deaerated by high-purity argon for 2 h prior to any measurement. For linear sweeping voltammetry and chronoamperometry of formic acid oxidation, the electrolyte solution was 1 M formic acid in 0.5 M H_2SO_4, which was prepared from high-purity sulfuric acid, high-purity grade formic acid, and distilled water.

For the electrochemical measurement of the adsorbed CO on Pd/C and PdRu/C catalysts, CO was bubbled into the solution for 10 min when the electrode potential was fixed at 0 V vs. Ag/AgCl. Then, Ar was bubbled into the solution for 10 min to remove CO in the solution. No background subtraction in linear seeping voltammetry was used.

Results and discussion

The typical TEM images of the Pd_3Ru_1/C, Pd_1Ru_1/C and Ru/C catalysts are shown in Fig. 1. As shown in Figs. 1a, b, and c, a remarkably uniform and high dispersion of metal particles on the carbon surface with an average diameter of 4.2, 3.9, and 4.9 nm for Pd_3Ru_1/C, Pd_1Ru_1/C and Ru/C, respectively. Evidently, Pd_3Ru_1/C, Pd_1Ru_1/C and Ru/C nanoparticles, synthesized by a microwave-assisted polyol process, present well-dispersed particles on Vulcan XC-72 and relatively narrow particle size distributions as shown in Figs. 1d, e, and f. To determine the actual palladium and ruthenium contents in the PdRu alloys, inductively coupled plasma spectroscopy was used to measure the unreacted metal ions remaining in the ethylene glycol mixtures. The PdRu alloy nanoparticles of compositions of $Pd_{5.4}Ru_1$, $Pd_{3.3}Ru_1$ and $Pd_{1.4}Ru_1$ were obtained from precursors of Pd_5Ru_1, Pd_3Ru_1 and Pd_1Ru_1. The analyses indicate that there were some deviations from the targeted compositions.

The power XRD patterns for PdRu/C are shown in Fig. 2 alongside the diffraction patterns of a Pd/C catalyst used as comparison. The diffraction peak at 20–25° observed in all the XRD patterns of the carbon-supported catalysts is due to the (002) reflection of the hexagonal structure of Vulcan XC-72 carbon. For Ru/C catalyst, the peaks at 44°, 58°, 69°, and 78° can be respectively assigned to the (101), (102), (110), and (103) planes of a Ru hexagonal closed-

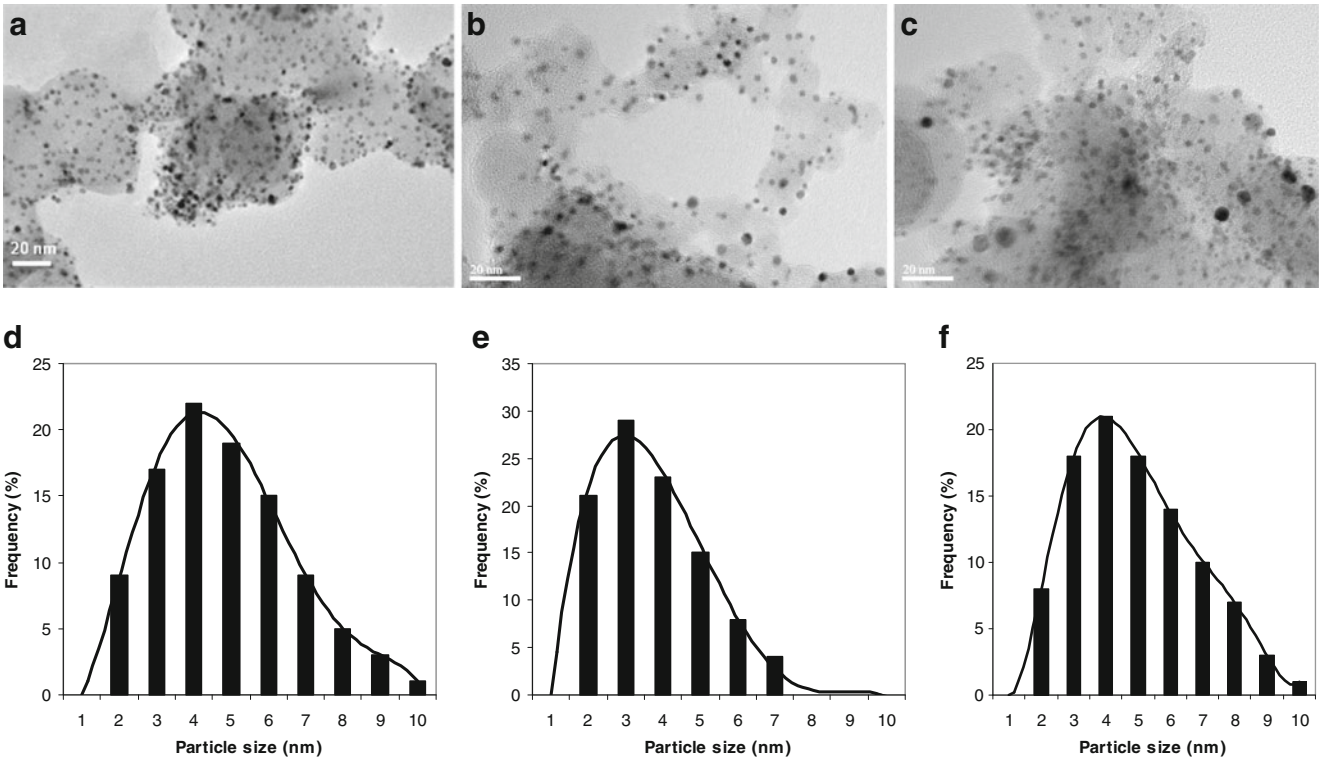

Fig. 1 TEM images (**a**, **b**, and **c**) and histograms of particle size distribution (**d**, **e**, and **f**) of Pd_3Ru_1/C, Pd_1Ru_1/C and Ru/C catalysts

packed lattice. For Pd/C and PdRu/C catalysts, the diffraction peaks at about 40°, 47°, 68°, and 82° are due to the Pd (111), (200), (220), and (311) reflections, respectively, which represents the typical character of a crystalline Pd face-centered cubic (fcc) phase. This indicates that the Ru was either in an amorphous state or alloyed with the Pd. There are no other distinct reflection peaks in all spectra than those of the four peaks mentioned above, indicating that these electrocatalysts have prevailed

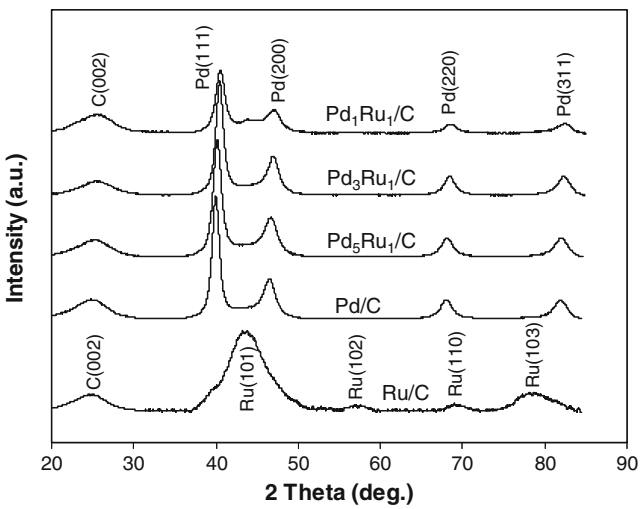

Fig. 2 XRD patterns of PdRu/C and Ru/C catalysts

Pd (fcc) crystal structure. Careful investigation of Fig. 2 reveals that all diffraction peaks were shifted synchronously to higher 2θ values with increasing Ru concentration in the catalysts. The shift was an indication of the reduction in lattice constant. The lattice parameters of Pd, Pd_5Ru_1, Pd_3Ru_1, and Pd_1Ru_1 were 3.911, 3.906, 3.892, and 3.885 Å, respectively. According to Vegard's law [22], the lattice constant was usually used to measure the extent of alloying:

$$a_{\mathrm{PdRu}} = a_{\mathrm{Pd}} - kx_{\mathrm{Ru}} \quad (1)$$

where a_{Pd}=3.911 Å is the lattice parameter of pure Pd, a_{PdRu} is the lattice parameter of PdRu alloy, and k=0.124 Å is a constant. From the values of lattice parameters, we have calculated Ru atomic fraction in PdRu alloy. The value of x_{Ru} for Pd_5Ru_1, Pd_3Ru_1, and Pd_1Ru_1 are 0.04, 0.15, and 0.21, respectively. The reduction of lattice constant primarily arose from substitution of palladium atoms with Ru atoms, resulting in contraction of the fcc lattice, which indicated the formation of the PdRu alloy.

The linear sweeping voltammograms of 1 M HCOOH in 0.5 M H_2SO_4 solution at the different catalysts are shown in Fig. 3. The most commonly accepted mechanism is the so-called "parallel or dual pathway mechanism" [23, 24], which involves the following formal reaction pathways [Eqs. (2) and (3)]:

$$\mathrm{HCOOH} \rightarrow \mathrm{CO_2} + 2\,\mathrm{H^+} + 2\,\mathrm{e^-} \quad (2)$$

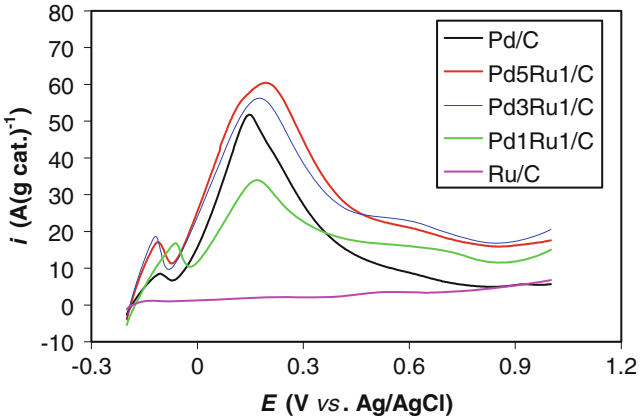

Fig. 3 Linear sweeping voltammograms of Pd/C and PdRu/C catalysts in 1 M HCOOH, 0.5 M H_2SO_4 with a scan rate of 50 mVs^{-1} at 25 °C

$$HCOOH \rightarrow CO_{ad} + H_2O \text{ and} \quad (3a)$$

$$H_2O \rightarrow OH_{ad} + H^+ + e^- \text{ and} \quad (3b)$$

$$CO_{ad} + OH_{ad} \rightarrow CO_2 + H^+ + e^- \quad (3c)$$

The first pathway [Eq. (2)] was denoted as a direct pathway, while the other set of reactions [Eqs. (3a)–(3c)] was described as the indirect pathway. All voltammograms refer to the features in the third cycle, where steady-state response was obtained. There was no significant feature difference between the linear sweeping voltammogramms of room temperature formic acid on carbon-supported Pd and carbon-supported PdRu catalysts. Obviously, no anodic peak was observed at the Ru/C catalyst, indicating that the Ru/C catalyst has no electrocatalytic activity for the oxidation of formic acid. It can be observed that there is a large peak near 0.2 V corresponds to formic acid oxidation. Compared with Pd/C electrode, the current densities of the anodic peak of formic acid oxidation are different at different PdRu/C electrodes. They are 52, 61, 56, and 35 $A(g\ cat.)^{-1}$ at the Pd/C, Pd_5Ru_1/C, Pd_3Ru_1/C and Pt_1Ru_1/C catalysts, respectively, indicating that the electrocatalytic activity of the Pd_5Ru_1/C catalyst for the oxidation of formic acid is the highest among all the catalysts. When the mole ratio of Pd and Ru was 5:1 and 3:1, the electrocatalytic activity of the PdRu/C catalyst for the oxidation of formic acid was better than that of the Pd/C catalyst. However, when the mole ratio of Pd and Ru was increased to 1:1, i.e., Pt_1Ru_1/C, the electrocatalytic activity was worse than that of the Pd/C catalyst because Ru has no electrocatalytic activity for the oxidation of formic acid.

The linear sweeping voltammograms of the Pd_3Ru_1/C catalyst in 0.5 M H_2SO_4 solution containing 1 M formic acid at different scan rates are shown in Fig. 4. It can be clearly seen in Fig. 4 that the peak potential shifts positively with the increase in the scan rate, which indicates that the electrocatalytic oxidation of formic acid at the Pd_3Ru_1/C catalyst electrode is an irreversible electrode process. In the case of an irreversible reaction, the peak current is [25, 26]

$$i_p = 2.99 \times 10^5 n(\alpha n')^{1/2} C_\infty D^{1/2} v^{1/2} \quad (4)$$

where n is the electron number for the total reaction, n' is the electron number transferred in the rate-determining step, α is the charge transfer coefficient, i_p is the peak current density (Ampere per square centimeter), D is the diffusion coefficient (centimeters per second), C_∞ is the formic acid concentration (moles per cubic centimeter) in the solution and v is scan rate (Volts per second). The peak current increases linearly with the square root of the scan rates as shown in Fig. 4 insert. The peak potential values for the irreversible system are proportional to the log v as the following equation at 25 °C [25]

$$\left|dE_p/d\log v\right| = 29.6/(\alpha n')(\text{mV}) \quad (5)$$

where E_p is the peak potential (millivolts) and v is the scan rate (Volts per second). The dependence of the peak potential on log v is shown in Fig. 5. The slope is 110 mV. Thus, the value of $\alpha n'$ is 0.27 obtained from Eq. (5). A common concept in electrochemistry is that elementary electron-transfer reaction always involves the exchange of one electron, so that an overall process involving a change in n electrons must involve n distinct electron-transfer steps [27]. Within this view, a rate-determining electron transfer is always a one-electron process, $n'=1$, $\alpha=0.27$. The low values of $\alpha=0.27$ indicated the slow kinetic process for formic acid oxidation at the PdRu catalyst electrode. Further

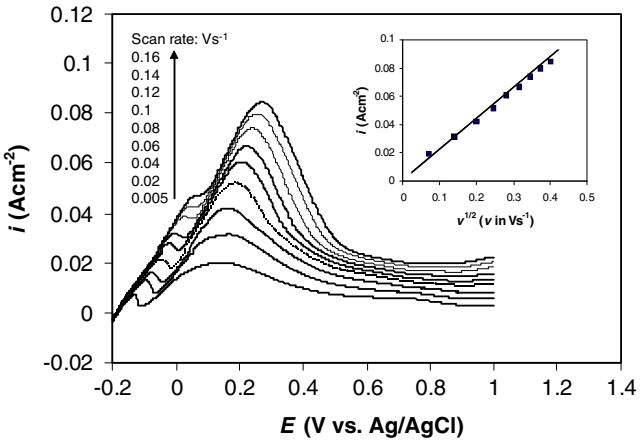

Fig. 4 The linear sweeping voltammograms of the Pd_3Ru_1/C catalyst in 1 M HCOOH, 0.5 M H_2SO_4 with different scan rates at 25 °C

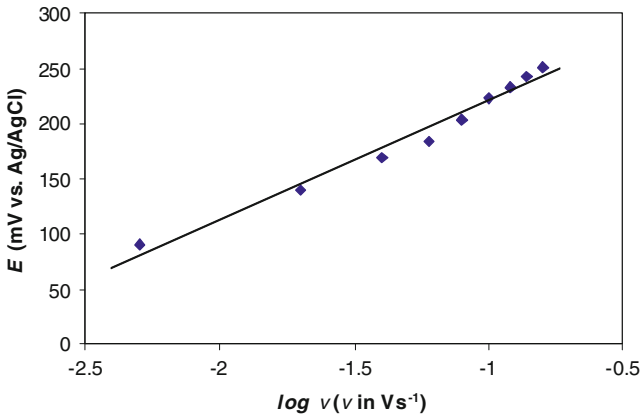

Fig. 5 The peak potential vs. log v of the Pd_3Ru_1/C catalyst in 1 M HCOOH, 0.5 M H_2SO_4 at 25 °C

studies are needed in order to identify the rate-determining step in the multistep mechanism of Eq. (3a) to Eq. (3c). The value of diffusion coefficients, D, can be obtained from the slopes of the lines in Fig. 4 insert. The D value is a measurement of the charge-transport rate within the liquid film near the electrode surface. The value of D is 5.52×10^{-6} cm^2 s^{-1} for Pd_3Ru_1/C catalyst electrode. The same pattern of peak current density vs. the square root of the scan rate and peak potential vs. the logarithm of the scan rate on the Pd/C catalyst electrode was observed. The value of D (2.67×10^{-6} cm^2 s^{-1}) is slightly lower for Pd/C catalyst electrode compared with Pd_3Ru_1/C catalyst electrode but with the same order of magnitude. This suggests that higher electrocatalytic activity of Pd_3Ru_1/C catalyst electrode is not attributed to the change of diffusion coefficient. Changing these diffusion coefficients revealed for cases of different electrodes may be associated with difference in the real surface area of the electrodes.

Pd/C and PdRu/C catalysts were biased at 0.3 V vs. Ag/AgCl and the changes in their polarization currents with time were recorded (Fig. 6). The pattern of current decay was different for each catalyst. For the Pd/C catalyst, the current decayed continuously even after 0.5 h, supposedly because of catalyst poisoning by the chemisorbed carbonaceous species. The Pd_5Ru_1/C is able to maintain the highest current density for over 0.5 h among all the catalysts, indicating enhanced electrocatalytic activity compared with Pd/C and other PdRu/C catalysts. The comparative tests concluded that Pd_5Ru_1/C had the best electrocatalytic performance among all carbon-supported Pd based catalysts prepared in this paper. The rate of current decay also varied between catalysts, with PdRu/C showing faster decay, while the current at Pd/C became quite stable after an initial rapid decay. The reason will be further investigated in future.

In order to evaluate the CO buildup on different catalysts, CO-stripping linear sweeping voltammograms of the adsorbed CO in 0.5 M H_2SO_4 solution at the different catalysts are shown in Fig. 7. It was observed that no anodic peak appears at the Ru/C catalyst, indicating that CO cannot be adsorbed on the Ru surface. The most notable difference between CO-stripping on PdRu/C catalysts and Pd/C catalyst is the negative shift of the CO oxidation peak in the former case. At the Pd/C catalyst, a strong anodic peak of adsorbed CO is located at 0.76 V. However, at the PdRu/C catalysts, the anodic peaks of the adsorbed CO are located between 0.71 and 0.73 V, which are more negative than that at the Pd/C catalyst. This is an indication that addition of Ru is helpful to weakening the adsorption strength of CO on Pd through the interaction between Pd and Ru. On the other hand, Ru can promote the oxidation of formic acid at Pd through the direct pathway because Ru can decrease the adsorption strength of CO. However, when the content of Ru in the PdRu/C catalyst is too high, the electrocatalytic activity of the PdRu/C catalyst would be decreased because Ru has no electrocatalytic activity for the oxidation of formic acid.

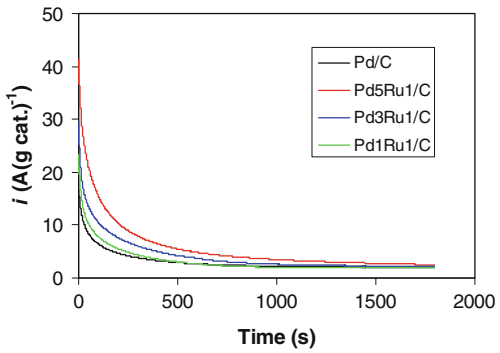

Fig. 6 Polarization current vs. time plots for the electrooxidation of formic acid in 1 M HCOOH, 0.5 M H_2SO_4 electrolyte at 0.3 V (vs. Ag/AgCl) at 25 °C

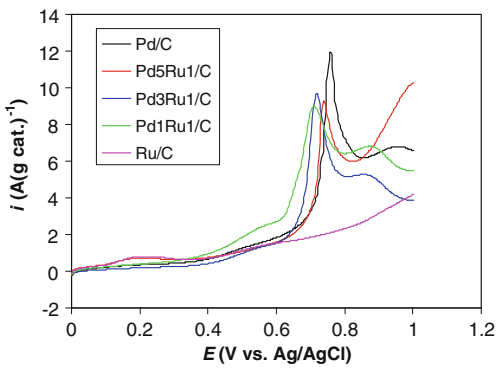

Fig. 7 CO-stripping linear sweeping voltammograms on Pd/C and PdRu/C catalysts in 0.5 M H_2SO_4 with a scan rate of 50 mVs^{-1} at 25 °C

Conclusions

Pd and PdRu nanoparticles supported on Vulcan XC-72 carbon were prepared by a microwave-assisted polyol process. The Pd and PdRu particles are nanoscopic-sized and have narrow particle size distributions. XRD analysis revealed that all PdRu catalysts displayed the characteristic diffraction peaks of a Pd fcc crystal structure, but the 2θ values were all shifted to slightly higher values. Some PdRu alloy catalysts, especially the bimetallic system of Pd_5Ru_1/C, showed excellent catalytic activities for electro-oxidation of formic acid. This is attributed to that addition of Ru is helpful to weakening the adsorption strength of CO on Pd through the interaction between Pd and Ru.

References

1. Dillon R, Srinivasan S, Aricò AS, Antonucci V (2004) J Power Sources 127:112
2. Rice C, Ha S, Masel RI, Waszczuk P, Wieckowski A, Barnard T (2002) J Power Sources 111:83
3. Rice C, Ha S, Masel RI, Wieckowski A (2003) J Power Sources 115:229
4. Wang X, Hu JM, Hsing IM (2004) J Electroanal Chem 562:73
5. Xia X, Iwasita TJ (1993) J Electrochem Soc 140:2559
6. Jarvi TD, Stuve EM (1998) Fundamental aspects of vacuum and electrocatalytic reactions of methanol and formic acid on platinum surfaces (Chapter 3). Wiley, NY
7. Markovic N, Gaseiger H, Ross P, Jian X, Villegas I, Weaver M (1995) Electrochim Acta 40:91
8. Jiang J, Kucernak A (2002) J Electroanal Chem 520:64
9. Park S, Xie Y, Weaver MJ (2002) Langmuir 18:5792
10. Lovic JD, Tripkovic AV, Gojkovic SL, Popovic KD, Tripkovic DV, Olszewski P, Kowal A (2005) J Electroanal Chem 581:294
11. Capon D, Parsons R (1975) J Electroanal Chem 65:285
12. Arenz M, Stamenkovic V, Schmidt TJ, Wandelt K, Ross PN, Markovic NM (2003) Phys Chem Chem Phys 5:4242
13. Ha S, Larsen R, Zhu Y, Masel RI (2004) Fuel Cells 4:337
14. Ha S, Larsen R, Masel RI (2005) J Power Sources 144:28
15. Shobha T, Aravinda CL, Bera P, Devi LG, Mayanna SM (2003) Mater Chem Phys 80:656
16. Kibler LA, El-Aziz AM, Kolb DM (2003) J Mol Catal A Chem 199:57
17. Jayashree RS, Spendelow JS, Yeom J, Rastogi C, Shannon MA, Kenis PJA (2005) Electrochim Acta 50:4674
18. Wang X, Tang Y, Gao Y, Lu T (2008) J Power Sources 175:784
19. Yu WY, Tu WX, Liu HF (1999) Langmuir 15:6
20. Komarneni S, Li DS, Newalkar B, Katsuki H, Bhalla AS (2002) Langmuir 18:5959
21. Liu ZL, Guo B, Hong L, Lim TH (2006) Electrochem Commun 8:83
22. Gasteiger HA, Ross PN, Cairns EJ (1993) Surf Sci 293:67
23. Chen YX, Heinen M, Jusys Z, Behm RJ (2007) Chemphyschem 8:380
24. Chen YX, Heinen M, Jusys Z, Behm RJ (2006) Angew Chem Int Ed 45:981
25. Brett CMA, Brett MO (2002) Electrochemistry (Part II). Oxford University Press, Oxford
26. Wang Y, Wu B, Gao Y, Tang Y, Lu T, Xing W, Liu C (2009) J Power Sources 192:372
27. Bard AJ, Faulkner LR (2000) Electrochemical method. John Wiley & Sons Inc, New York